Calorimeter analysis at the DELPHI experiment

Stefan Ask

Department of Mechanical Engineering
Division of Physics

Preface

The DELPHI experiment is one of the four experiments at LEP[1], the largest particle accelerator at the European Laboratory for Particle Physics, CERN, in Switzerland.

During the summer of 1999 I participated as a summer student in a group at the DELPHI experiment at CERN. The "Summer Student Programme" invites undergraduate students that have completed at least three years of fulltime university studies. I spent thirteen weeks at CERN, where 75% of the time consisted of research and 25% of lectures in particle physics related subjects. After this I returned to Luleå to finish my master's thesis.

The group I was working with made a so-called single-photon analysis and it was in connection with this analysis I did a study of the DELPHI calorimeters. The study used both real DELPHI data and Monte Carlo simulations of the DELPHI experiment.

During the summer, the group also performed a test run of a new calorimeter prototype, called Caleido, to verify if a new detector technique could be used at a future e^+e^- accelerator.

The results of my study were presented at the weekly DELPHI meeting, called the forum and some of the results were presented by DELPHI physicists at four other DELPHI meetings. A peer-reviewed DELPHI note was also written, which included some of the work presented in this thesis.

[1] Large Electron Positron collider

Abstract

This master's thesis discusses a study of the background in the DELPHI calorimeters together with an evaluation of a Monte Carlo simulation of a counter detector connected to one of the calorimeters, called the veto counter. A new calorimeter prototype will be discussed as well.

The background study was made by using a so-called random trigger. The random trigger is well suited for this purpose and the study is of special interest for the STIC calorimeter, which suffers a lot of background since it is placed closest to the beam pipe.

The evaluation of the veto counter simulation was made to see if a recently improved Monte Carlo simulation was accurate enough to be used in a real physics analysis.

Keywords: DELPHI calorimeters, STIC, Background, Random trigger, Veto counter, Monte Carlo simulation.

Acknowledgement

First of all I want to thank my supervisor at CERN, Vincent Hedberg, who gave me the opportunity to work with this project. I am especially grateful for all the help I got with the particle physics and regarding detector construction. I also want to thank my supervisor and examiner in Luleå, Sverker Fredriksson, for encouraging me to this MSc diploma work. Finally, I want to thank Per Arve and Jonas Lundberg who recommended me as a participant in the summer student programme.

Contents

Chapter 1

Introduction

In this report a study of the calorimeters[1] in the DELPHI experiment at CERN is presented. The study mainly concerns the STIC detector, which is an electromagnetic calorimeter for measuring the luminosity[1] of the LEP accelerator. The study was a part of the single photon analysis, in which one looks for collisions with only one photon and no other particles detected in the experiment. The so-called off-energy electron background in the STIC detector was studied as well asthe noise in the other calorimeters. An off-energy electron is an electron in LEP, which is, scattered on a gas molecule in the beam pipe into the detector.

In addition to the DELPHI study, a 1999 test run of CALEIDO, a detector prototype similar to STIC, will be discussed.

My work consisted of two parts, and the first one was the Random trigger[1] analysis. It was a measurement of background and noise in the calorimeters in the DELPHI experiment with random triggers. These triggers give a background sample without any signals from a real LEP interaction. The study was made for all the calorimeters in the DELPHI experiment, but with emphasis on the STIC detector.

According to results from earlier studies, one expected off-energy electrons to be the main background in the STIC detector. The off-energy electrons have been simulated in the DELPHI experiment, but the simulation could not be used for quantitative estimations since it needs as input the vacuum pressure in the beam pipe, which is not known in detail. The random trigger analysis, on the other hand, has never been used in DELPHI before, and since it is an analysis with real data it suits the study of off-energy electrons well.

The off-energy electrons only hit the STIC calorimeter since it is situated closest to the beam pipe, and this is one of the reasons why the analysis was concentrated on STIC. The main questions to be answered by this study were:

- *Is the background in STIC dominated by off-energy electrons?*
- *What is the probability for an off-energy electron to give a signal in the STIC detector in an arbitrary event?*
- *What is the probability for a signal caused by noise or background in any of the other calorimeters in DELPHI in an arbitrary event?*

The second part of my study was an evaluation of a Monte Carlo simulation[1] of the veto counter. The veto counter is a detector consisting of scintillators[1] used for identifi-

[1]See glossary in Appendix A.

cation of particles, and it is a part of the STIC detector. Monte Carlo simulations of this detector have been made before but with poor agreement with the real veto counter data. Monte Carlo simulations are a crucial tool in many analyses for to estimates of different backgrounds, and that is why this Monte Carlo simulation programme was improved just before I arrived at CERN. The question to be answered by this study was:

- *Is the Monte Carlo simulation of the veto counter accurate enough to be used in a real physics analysis?*

In both parts of my study, high-energy data recorded during the 1998 and 1999 LEP runs have been used.

Chapter 2

The LEP accelerator

The Large Electron Positron, LEP, collider is the largest accelerator at CERN. LEP is a synchrotron accelerator and has a circular storage ring with a circumferense of 27 km, in which the electrons and positrons are guided. The electrons and positrons are accelerated in bunches, and because it is particles and anti-particles that are used in the LEP collider they can be accelerated in the same beam pipe and bent by the same magnets (see figure 2.1). In the beam pipe it is necessary to have a high vacuum so that few interactions between residual gas molecules and the electrons and positrons will take place. The collisions occur at four different places along the accelerator ring. The bending of the beams in synchrotron accelerators gives rise to synchrotron radiation, or *Bremsstrahlung*. Due to this it is an advantage to have a radius that is as large as possible to get as little energy as possible radiated away from the particles.

LEP is located 100 metres below ground and contains 4184 magnets. The usage of LEP, since its start in 1989, consists of two phases, LEP1 and LEP2. LEP1 is the running of LEP from 1989 until 1995, when the highest centre of mass energy was just above the Z^0-particle mass, $\sqrt{s} = m_Z$. LEP2 corresponds to the period 1995-2000, and during this period the energy has been increased in stages, with the first stage at $\sqrt{s} = 130$ GeV and the last at 204 GeV. The first goal at LEP2 was to reach the centre of mass energy equal to twice the W-particle mass, which was reached in 1996. After this the energy has been increased each year to get the maximum energy out of the machine before it will be shut down permanently after the summer of 2000. The maximum energies are of great importance in many searches for new particles since LEP is the largest accelerator of its kind. The LEP accelerator is used only during the summer when electricity is cheap, since it consumes as much power as about 40% of the city of Geneva.

The electrons and positrons are injected into LEP after being accelerated by five different accelerators up to 20 GeV. First the electrons and positrons are created by an electron gun and a positron converter, and then accelerated by a linear accelerator to 200 MeV. After that they are further accelerated by another linear accelerator up to 600 MeV and then transfered to a 600 MeV electron-positron accumulator, the EPA (see figure 2.2). The electrons and positrons are then accelerated in the Proton Synchrotron, PS, to 3.5 GeV. Finally the electrons and positrons are accelerated by the Super Proton Synchrotron, SPS, to 20 GeV. After SPS, the electrons and positrons are injected into LEP and are accelerated up to an energy of 102 GeV (which was reached at the end of the summer of 1999). The two proton synchrotrons used as pre-accelerators to LEP run in so-called multicycle mode. They accelerate four cycles of electrons and positrons and

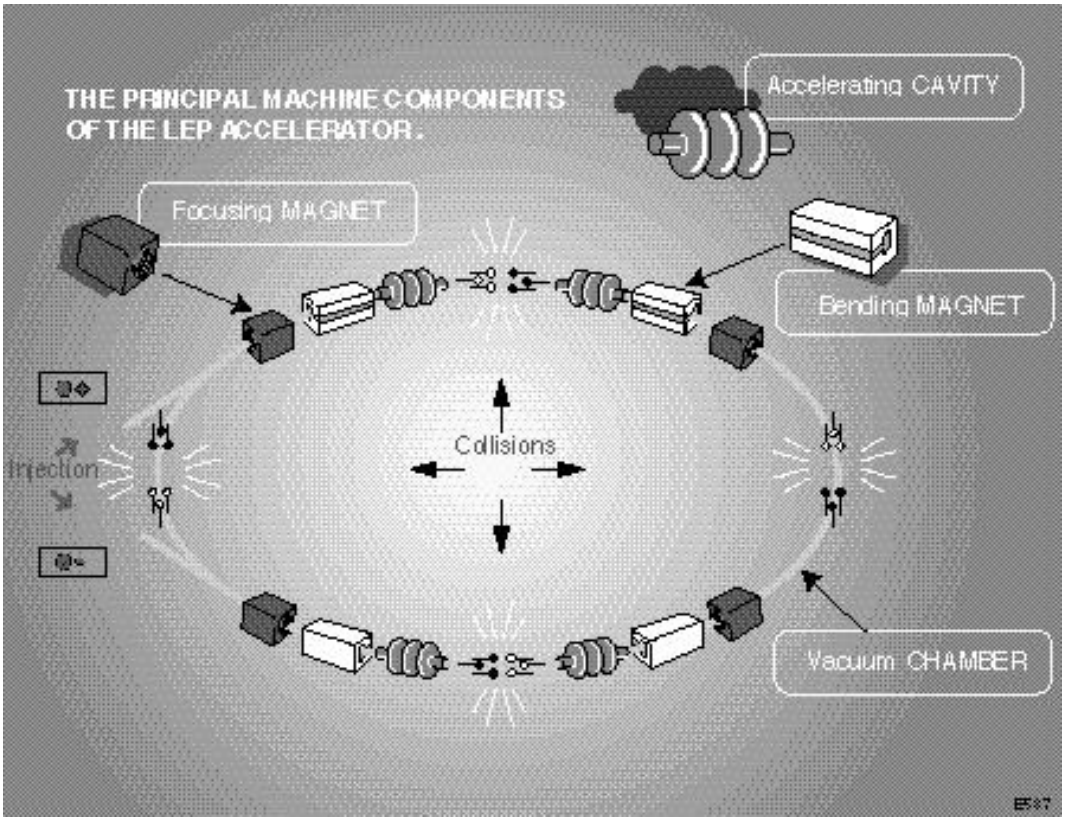

Figure 2.1: Overview picture of the LEP collider.

then one cycle of protons. When the electrons and positrons are accelerated between the proton cycles they do not disturb the proton beams in the SPS.

Strings of dipole magnets are used to bend the beams in piecewise circular trajectories along the approximately circular beam pipe. Dipole magnets are also used for vertical and horizontal corrections of the beams. Quadrupole and sextupole magnets are used to focus the beams and to cancel out oscillations of the electrons and positrons. At the collision points superconducting quadrupole magnets are used to focus the beams very tightly. There the beams have a vertical width of about 10 μm and a horizontal width of about 250 μm.

The acceleration of the particles is made with so-called Radio Frequency (RF) cavities (see figure 2.3). The RF-cavity is a resonator construction which provides a maximum acceleration, by a time-varying electromagnetic field, at the same time as the power loss is minimized due to its resonator properties. To achieve this, the RF-cavity consists of two coupled cavities, one copper cavity in which the particles are accelerated and one low-loss cavity where the electromagnetic power is stored half of the time to minimize the power loss due to heating of the copper cavity. The electromagnetic energy oscillates between the two cavities with a frequency of about 352 MHz, which corresponds approximately to 31 times the frequency of the beam circulating LEP. Since the energy peak appears about 31 times per revolution this is also the number of bunches possible to accelerate. The particles are supposed to collide at very specific locations and must be accelerated at specific moments in the cavities. This requires a very precise synchronization between the LEP RF-system and the SPS injector.

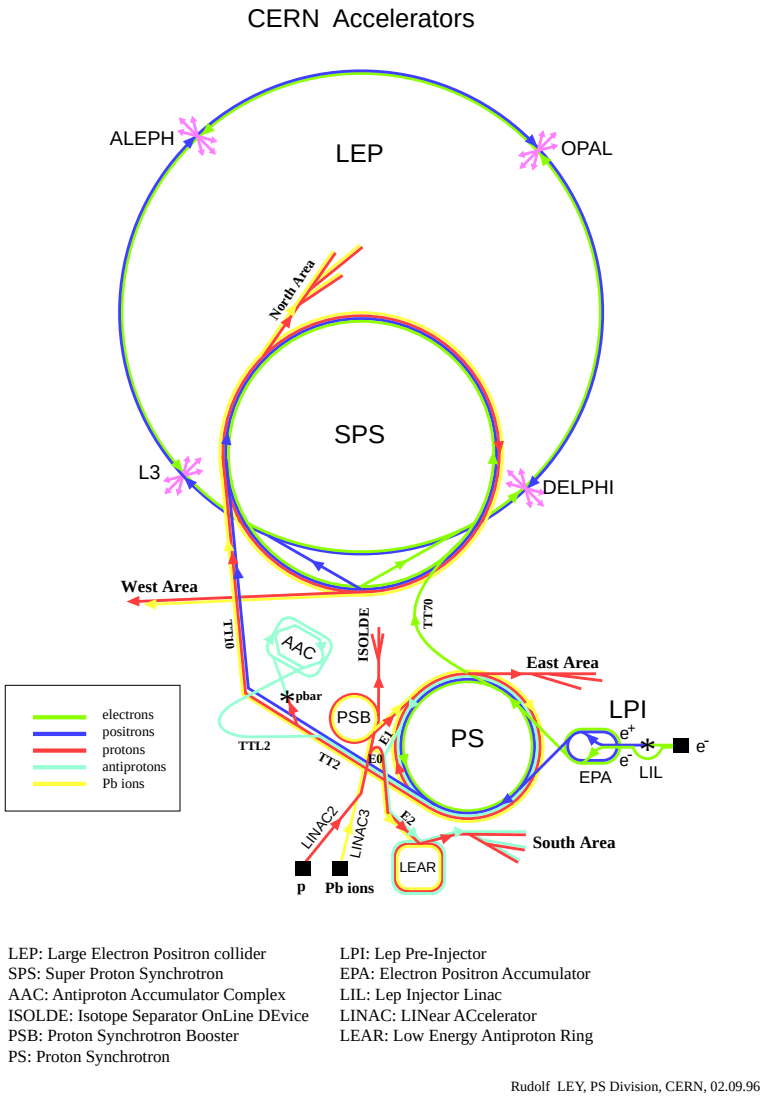

Figure 2.2: Overview picture of the accelerator complex.

The beam energy in LEP is very accurately determined, and at $\sqrt{s} = m_Z$ the error was about 0.002 GeV, but it is also sensitive to disturbances. Because of the Lorentz force that bends the beam, and the fact that the beam energy is approximately equal to the momentum at these energies, the beam energy is related to the length around LEP as

$$\frac{d\overline{p}}{dt} = q\overline{v} \times \overline{B} \text{ and } E \cong p \Rightarrow E_{beam} = \frac{e}{2\pi} \oint_{LEP} \overline{B} \cdot \overline{dl}.$$

When the magnetic field is fixed, the result is that deformations of the LEP ring due to geological phenomena can affect the LEP energy significantly compared to the accuracy of LEP. A Δl stretch of $\mathcal{O}(10^{-4}\text{m})$ of the LEP ring results in a ΔE of $\mathcal{O}(\text{MeV})$. Because of the sensitivity of LEP, correlations have been measured between LEP and, among other things, the moon and the water level of lake Geneva. Also other disturbances than deformations of the LEP ring have been detected, such as leakage currents from nearby railways, which follow the beam pipe and affect the magnetic field in the magnets.

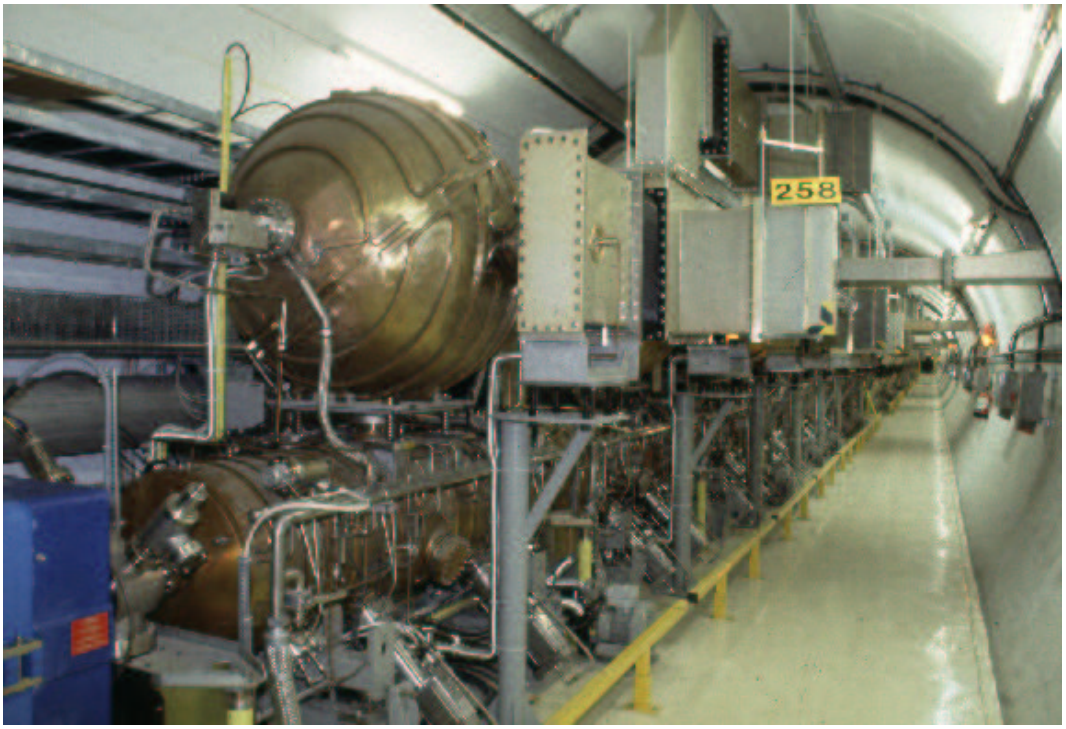

Figure 2.3: Picture of an RF-cavity in the LEP tunnel.

Chapter 3

The DELPHI experiment

The DELPHI experiment is one of the four experiments at the LEP collider. DELPHI stands for Detector with Lepton, Photon and Hadron Identification. It was installed together with the accelerator and has therefore been in use since 1989. The whole experiment is in the shape of a barrel with a 10 metre diameter and weighs about 3500 tons. This barrel consists of many different detectors, and about 550 physicists from 22 countries are working at the DELPHI experiment.

3.1 The structure of DELPHI

The electron and positron beams are forced together to collide in the middle of the DELPHI experiment. The experiment is constructed like an onion, where the different detectors are built in layers around the beam pipe, which gives the total shape of a large barrel (see figure 3.1). The experiment is hermetic, which means that no radiation escapes from the experiment, and that allows work near the DELPHI experiment when LEP is running. The order in which the different detectors are placed is chosen to make it possible to extract as much information as possible about the particles before they are destroyed by certain detectors. As can be seen in figure 3.1, the detectors are placed in the following order: Closest to the collision point are the tracking detectors and after them come the electromagnetic and the hadron calorimeters together with the scintillation counters. Finally, at the largest distance from the collision point are the muon chambers.

The tracking detectors use various techniques, but with the same main purpose, namely to detect how charged particles travel through the experiment and to measure their momentum. The tracking detectors do not destroy the particles, and that is the reason why they are placed closest to the beam pipe.

A typical tracking detector is the Time Projection Chamber (TPC, shown as a large cylinder in the centre of figure 3.1). The TPC contains a gas that becomes ionized when a particle travels through it. The chamber is divided in two separate cylinders with high voltage connected to their walls. These are in the plane perpendicular to the beam pipe, and the electrons and ions drift towards the walls when the gas is ionized. By measuring the time it takes for the electrons to drift to the TPC walls one can reconstruct the particle trajectory, since the drift velocity of the elecrons is known.

The electromagnetic calorimeters are placed in front of the hadron calorimeters because the hadrons get through the electromagnetic calorimeters, which is not the case for electrons and photons. This will be discussed in more detail below.

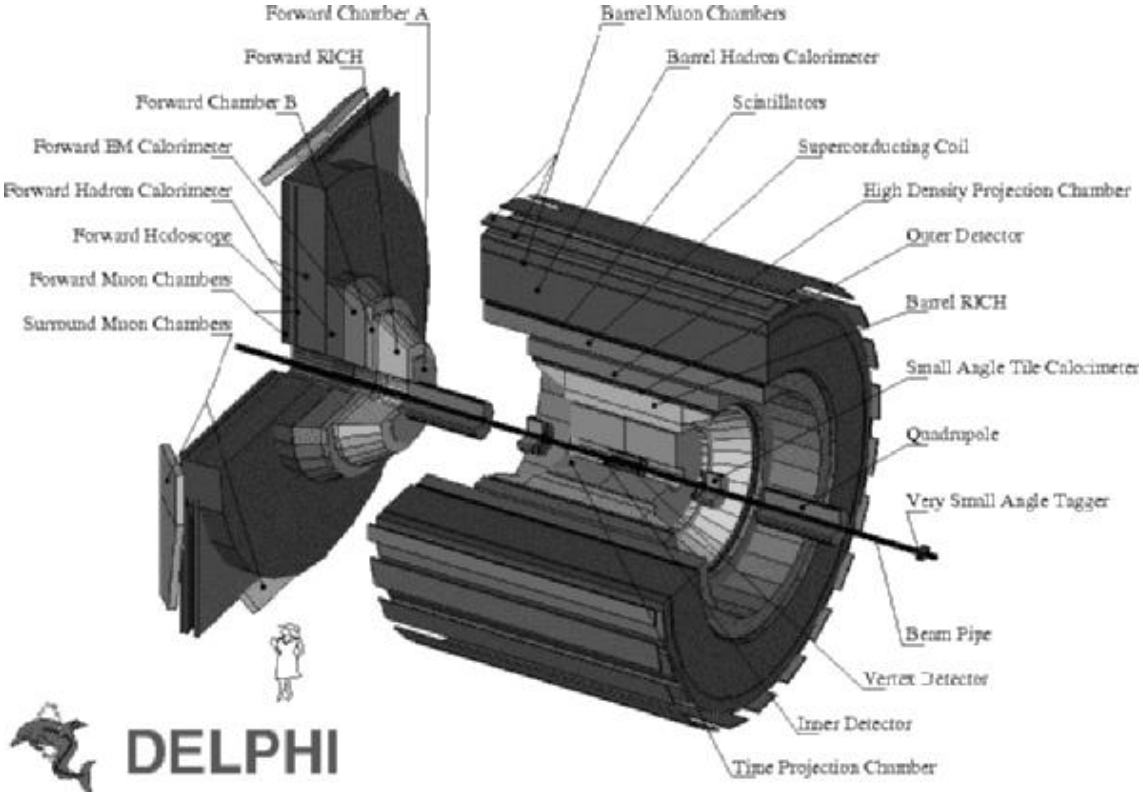

Figure 3.1: A general overview of the DELPHI detectors.

The muon chambers are located on the outside of the experiment since the muons are the only particles (with the exception of neutrinos) that can travel through the calorimeters, consisting partly of iron and lead, without showering.

3.2 The calorimeters

A calorimeter is a detector that determines the energy of a particle, but it can usually measure also other properties of the particle, such as direction etc. A calorimeter destroys the incoming particle. The DELPHI experiment has two types of calorimeters, and the first kind is the electromagnetic calorimeters. There are several such detectors. The first one is the High density Projection Chamber (HPC), which is the largest. It covers the barrel region. The second is the Forward ElectroMagnetic Calorimeter (FEMC) that covers the end areas of the barrel (called the endcaps). Apart from these two, there are two smaller calorimeters that are placed close to the beam pipe. Their main purpose is to measure the luminosity at LEP. They are called the Small angle TIle Calorimeter (STIC) and the Very Small Angle Tagger (VSAT, which is not used in this study). The two smaller calorimeters do not cover large areas, but are used to make precise measurements of certain events, so-called Bhabha events, with a cross-section that increases at lower angles. This will be discussed further in the STIC chapter. The DELPHI experiment also contains one hadron calorimeter called the HAdron Calorimeter (HAC). This calorimeter is located outside the electromagnetic calorimeters and covers both the barrel surface and the endcaps.

The principle is similar for electromagnetic and hadron calorimeters. The detector

uses chain reactions from the electron, photon or hadron when they go through a heavy material (usually lead) at high energies. When an electron (or photon) enters an electro-

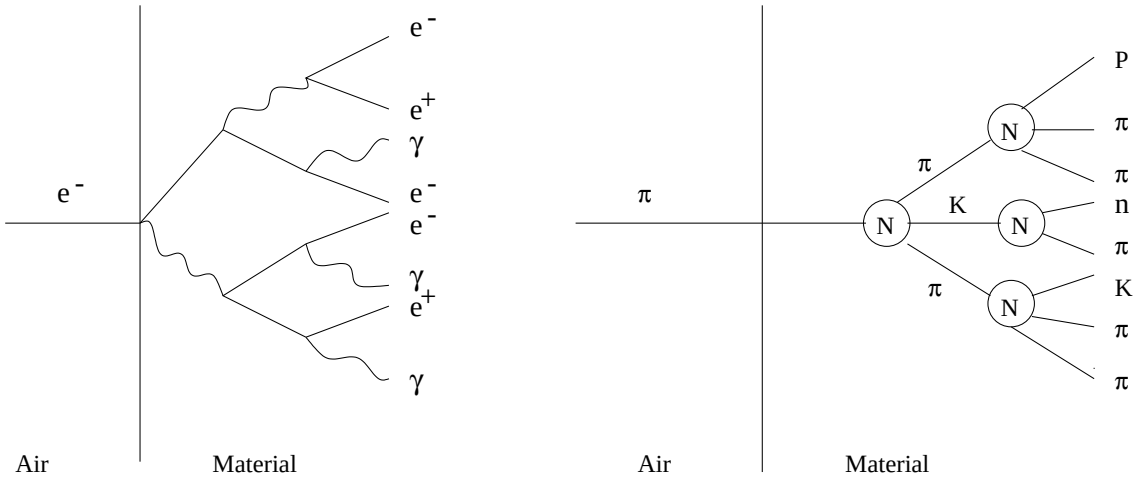

Figure 3.2: Left is shown a chain reaction, caused by bremsstrahlung and pair production, in an electromagnetic calorimeter. To the right one sees a typical hadronic chain reaction.

magnetic calorimeter at a high energy it interacts with the material. The atoms in the material make it possible for the electrons to radiate so-called *bremsstrahlung* and for the photon to produce electron-positron pairs, i.e., electromagnetic showers (figure 3.2). In this way a single electron or photon can produce new photons or electrons and so on. This chain reaction can be measured, in various ways, depending on how the detector is built, and the energy can be calculated. Such electromagnetic showers end when the energy of the individual electrons and photons has become too low to produce new particles. A typical electromagnetic shower in lead starts almost immediately after the particle has entered the detector material and is about 10 cm long and 2 cm wide.

The hadronic chain reaction is similar to the electromagnetic one. When a hadron enters the detector material it collides with the nucleons in the material and produces new hadrons that collides with new nucleons. This gives rise to hadronic showers, which end when the individual hadron energies have become small. A typical hadron shower in lead starts about 20-30 cm into the material and has a length of 1 m and a width of a couple of decimetres. This is the reason why the hadron calorimeters is behind the electromagnetic ones, as can be seen in the DELPHI figure 3.1.

HPC

The High density Projection Chamber is an electromagnetic calorimeter in the shape of a cylinder, and it consists of 144 independent modules. The angular coverage of the HPC is from 43 to 137 degrees. The modules, shaped like trapezoidal boxes, are mounted in six rings that build up the cylinder. In each module 41 lead plates are mounted with a 8 mm gap between them. These gaps are filled with a gas mixture of 20% methane and 80% argon. When an electron or photon enters HPC the showers are produced in the lead plates and the showers ionize the gas between the plates. Each module has a high voltage connected to its walls, which lies in the plane perpendicular to the beam pipe. When the gas is ionized the ions and electrons drift towards the walls due to the electrical

field. The size of the signal is proportional to the particle energy, and the time it takes for the electron cloud to travel to the walls is used to determine the impact point of the particle.

FEMC

The Forward ElectroMagnetic Calorimeter consists of two disks with a diameter of 5 m at each side of the barrel-shaped HPC. The FEMC covers the angles from 8 to 35 degrees and from 145 to 172 degrees. Each disk is made of 4532 lead glass blocks. The lead glass blocks look like truncated pyramids with a front area of 5.1×5.1 cm^2, a backside area of 5.6×5.6 cm^2 and a depth of 40 cm (figure 3.3). This is to get all the blocks to point at the collision point. The disks had to be tilted about one degree to ensure that particles travelling in straight trajectories are not able to escape in the insensitive regions between the blocks. The entering particles are able to interact with the lead glass and

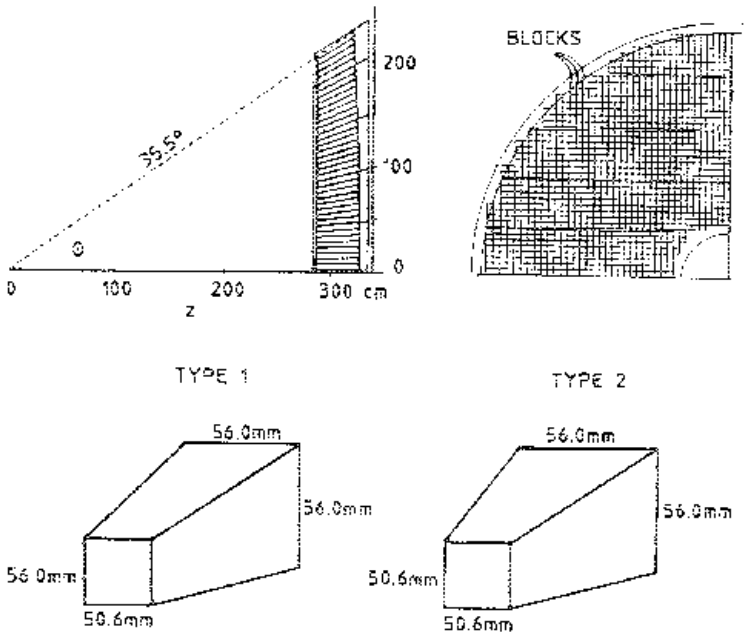

Figure 3.3: The FEMC lead-glass disks.

make electromagnetic showers. The electrons in the shower travel faster than light in the material and this forces them to emit so-called Cherenkov light. This light is collected by photodetectors, and the energy of the entering particle can be calculated.

HAC

The Hadron Calorimeter is a surrounding detector that contains three parts. It consists of one barrel part and two end disks. The barrel part of HAC covers angles from 42.6 to 137.4 degrees, and the two disks cover angles from 11.2 to 48.5 and 131.5 to 168.8 degrees. All the three parts are built by the same type of modules. The barrel part contains 24 modules and the end disks 12 each (figure 3.4). The modules are constructed in 20 layers (19 for the end parts) with 5 cm of iron and a 2 cm gap, where a detector is inserted, in each layer. The detector in the 2 cm gaps is a wire chamber of a so called limited streamer

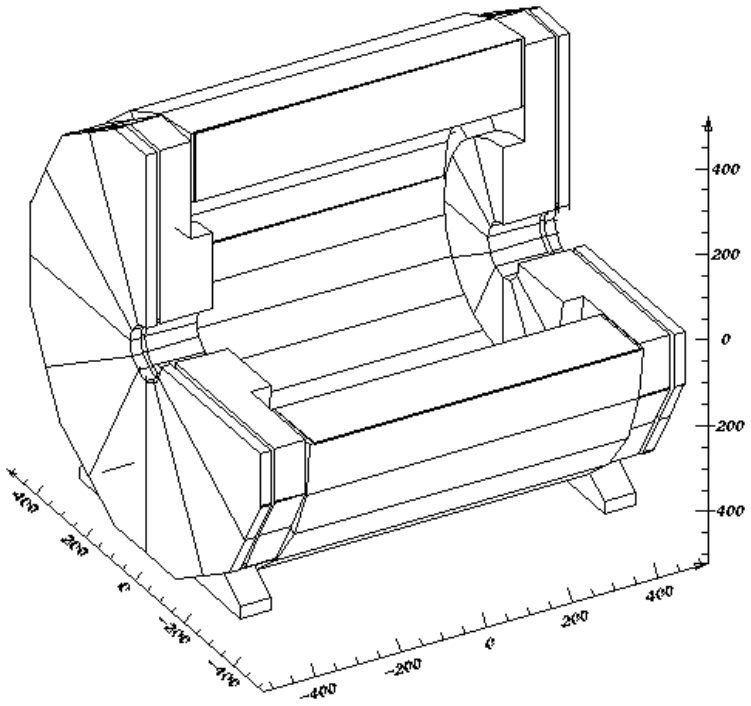

Figure 3.4: Illustration of the placement of the modules in HAC.

mode type. The wire chambers in HAC consist of plastic cathodes forming 8 cells in each detector, and an anode wire is inserted into each cell. The cathodes are coated with a low-conductivity graphite varnish. An electrical field is applied between the wire and the cathode, and the cells are filled with a gas mixture that becomes ionized when particles travel through it. Outside the cathode are copper-clad readout boards segmented into pads, which pick up signals from the ionization process (the streamers). The pads are arranged into towers that point to the interaction point. The energy, position etc of the particle that causes a shower, can be calculated within each such separate cell.

Chapter 4

The STIC and CALEIDO detectors

The Small angle TIle Calorimeter is an electromagnetic calorimeter used mainly for luminosity measurement at LEP, but it is also well suited for other studies. It was decided by the DELPHI collaboration in 1992 to build STIC and in 1994 the Small Angle Tagger (SAT) was replaced by STIC. Since the luminosity is measured by counting Bhabha events and the Bhabha cross-section increases at lower angles ($\frac{d\sigma}{d\theta} \propto \frac{1}{\theta^3}$), the STIC calorimeters were mounted as two half-cylinders almost directly around the beam pipe. With STIC as the luminometer, the luminosity measurement has an uncertainty of 0.09% at $\sqrt{s} = m_Z$. The STIC detector is built with a so-called shashlik technique, which makes STIC perfectly hermetic, and this property is of a great advantage in the search for new particles and was also one of the reasons for replacing the old luminometer. In addition to this shashlik calorimeter, two other detectors have been inserted. The first one is a silicon strip detector, which measures the direction of the particles and rejects some of the off-energy electron background. The other is a scintillation counter called the veto counter, which identifies electrons and photons. The veto counter is discussed in chapter 8.

4.1 Construction

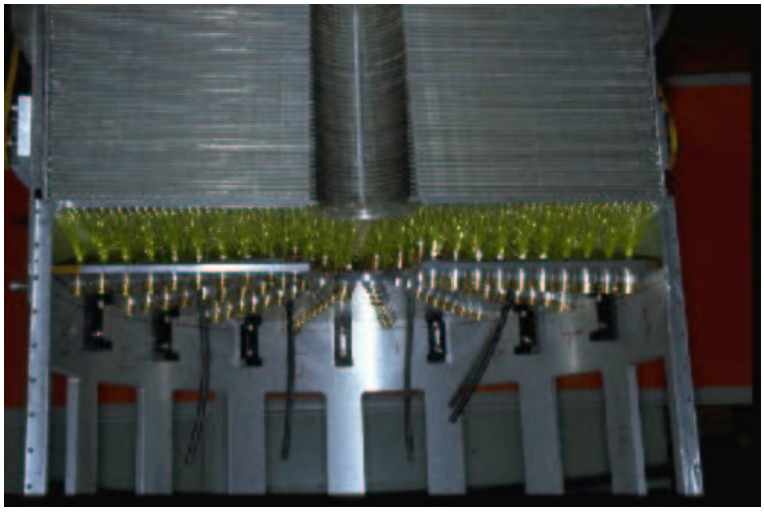

Figure 4.1: A cross-section of the STIC detector showing the lead-scintillator layers and the wavelength shifting fibers coming out from the towers.

The STIC detector consists of two cylinder-shaped calorimeters placed around the beam pipe at a distance of 2.2 m from the interaction point. Its angular coverage is from 1.7 to 10.6 degrees and from 169.4 to 178.3 degrees. The two STIC modules are lead-scintillator calorimeters and consist of 47 disk-shaped layers of 3 mm lead and 3 mm plastic scintillators (see figure 4.1). The light produced in the scintillators is guided by wavelength shifting fibers that run perpendicular to the lead-scintillator layers through holes made with very high precision. The layers have a total rotation from the first to the last layer of three degrees to prevent particles from travelling through the fiber holes and escape detection. Each layer of scintillators is divided into 10 rings and these rings are divided into 16 segments (figure 4.2). This gives the STIC calorimeters a so-called

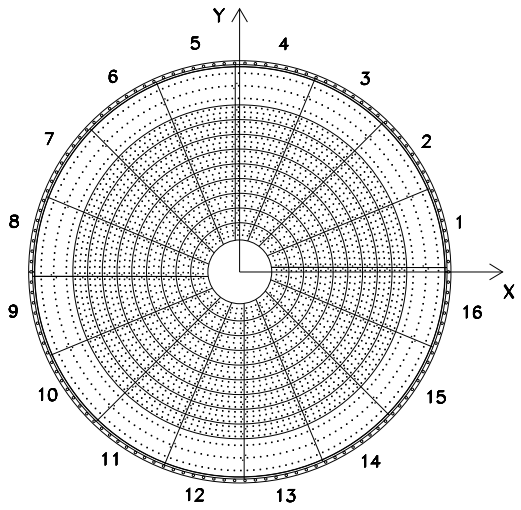

Figure 4.2: The STIC layers divided into a tower structure.

tower structure, where every piece of the divided disk becomes a part of a longitudinal lead-scintillator tower. The tower structure makes it possible to separate the showers and to determine a showers position. The light produced in the scintillators is read out by photomultipliers at the back of the STIC modules. Since the light produced by the scintillators is blue and the photomultipliers have a maximum sensitivity at green wavelength, one uses wavelength shifting fibers to be able to read out the light. All fibers from one tower is read out by the same photomultiplier.

4.2 Luminosity measurement with STIC

The STIC detectors main purpose is to measure the luminosity in LEP. The luminosity is a measure of the performance of the LEP collider, and it defines the collision rate in DELPHI. In a storage ring experiment it is the integrated luminosity that is of importance, i.e.,

$$\mathcal{L} = \frac{N}{\sigma} \ , \text{ where } \mathcal{L} = \int L(t)dt.$$

In this formula N is the number of detected events caused by a certain process and σ is the cross-section of this process. $L(t)$ is the luminosity at time t.

To minimize the statistical uncertainty of the calibration process one wants a large N-value. This implies that one needs to study a process with a large cross-section, which,

in addition, is theoretically well known. This suggests a process that can be described by pure QED (Quantum ElectroDynamics), which is a very accurate theory. The process selected to study the luminosity in LEP is the Bhabha scattering, $e^+e^- \rightarrow e^+e^-$, where the electron and positron are scattered mainly by the exchange of a photon. This process has a large cross-section, with very small corrections from the exchange of a Z^0-particle. The cross-section of the Bhabha scattering increases rapidly at lower angles, and this is why the luminometer (STIC) has to be placed as close as possible to the beam pipe. The cross-section of the Bhabha event is usually determined by Monte Carlo simulations. The uncertainty is of the order of 10^{-3}, and the main reason for this is the truncation of the perturbation series in the calcu lation.

To select the Bhabha events one requires so-called back-to-back Bhabha events with each shower energy being approximately $\frac{\sqrt{s}}{2}$. A back-to-back Bhabha event is when the electron and the positron trajectories from the collision point have an angle of about 180 degrees between them.

The largest source of systematic uncertainty of the luminosity, measured with STIC, is the distance between STIC and the interaction point. One has lowered this uncertainty through calculations of the trajectories connecting the showers from the Bhabha event. As the cross-section of Bhabha events depends so strongly on the polar angle is it very important to know the inner radius of STIC. This was achieved with a tungsten ring, called the W-nose, mounted at the inner radius of STIC. When particles enter STIC through the W-nose they lose most of their energy and the inner radius can then be well defined by an energy cut.

At LEP2 statistical limitations of the selected events made it unnecessary to measure the luminosity with as high accuracy as at LEP1. The W-nose was then removed and the inner radius was defined by a radial cut instead of the energy cut. After removing the W-nose this became the largest source of statistical uncertainty of the luminosity, but it was still in the order of 10^{-3}.

4.3 The CALEIDO project

The group I was working with performed a test run of a calorimeter prototype called CALEIDO. CALEIDO was a lead-scintillator calorimeter, read out with fibers, just like STIC, but with the difference that it had scintillators with different time response (figure 4.3). The idea with different time response was to be able to separate light that had been produced in the forward part of the calorimeter from light from the back. In this way one wanted to separate electrons from pions, since their showers appear differently in the calorimeter. CALEIDO was tested with a test beam at the west-side SPS area at CERN, and the test-run lasted six days. During this test period the group worked in shifts to use the test beam as much as possible. The CALEIDO detector was constructed very much like STIC. It was a lead-scintillator calorimeter consisting of 129 layers of 1 mm lead and 1 mm plastic scintillator. CALEIDO was also built with a tower structure containing 3×3 towers with a transverse dimension of 5×5 cm^2 each (figure 4.4). To prevent leakage in the towers, during the test run, the nine towers were surrounded by 16 towers from an earlier calorimeter prototype. The light produced in the scintillators was guided by wavelength shifting fibers, and the fibers were uniformly distributed with 25 fibers in each tower. The light in the fibers from each tower was read out by a photomultiplier at the

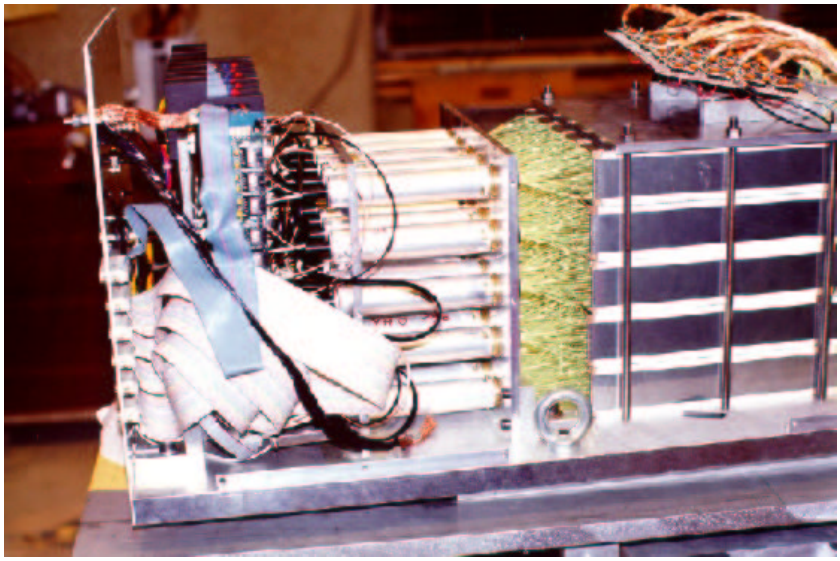

Figure 4.3: Side-view of CALEIDO showing the fibers coming out from the back and the photomultipliers in their cylinders.

back of CALEIDO. The towers were divided into two parts, which differed only in the time-response of the scintillators separating the electrons from pions. Showers caused by both types of particles appear in both of the sections, but the electron showers mainly appear in the front part of CALEIDO and the pions in the back. By using scintillators with a slower time-response in the first 29 layers of the towers one wanted to determine how much of the shower that appeared in the forward part compared to the back part.

At the west-side area the test run was performed in a shielded area were the beam was available. Apart of the SPS proton beam was used as test-beam and collided with various targets. For the electron beam a lead target was used and for the pion beam a copper target. After the collision between the SPS beam and the targets, particles of a certain type and with certain energies, directions, etc could be selected with a Cherenkov chamber together with various absorbers, magnets and collimaters. The change of beam was made from a terminal inside the control room. The testbeam setup is illustrated by figure 4.5. The beam first passed through two delay wire chambers (DWC). A delay wire chamber is a detector consisting of high voltage wires in a chamber with ionizable gas that gives a coordinate in the plane perpendicular to the beam when a charged particle has traveled through. The two delay wire chambers were used to determine the direction of the particles approaching CALEIDO. After the DWCs a scintillator counter (labeled S in figure 4.5) can be seen. This counter consisted of two crossed rectangular scintillators and was used as trigger, i.e., it indicated when a particle was going to enter CALEIDO and the measurement should start. CALEIDO was put on an adjustable table that could be moved vertically and horizontally from the control room.

An analysis of the data collected during the test-run showed good results. The signals from the different sections of CALEIDO were well separated and the separation between electrons and pions was possible. During the test-run electrons with 30 and 50 GeV were used as well as 50 GeV pions. In figure 4.6 the energy in the forward part of CALEIDO is plotted versus the total energy.

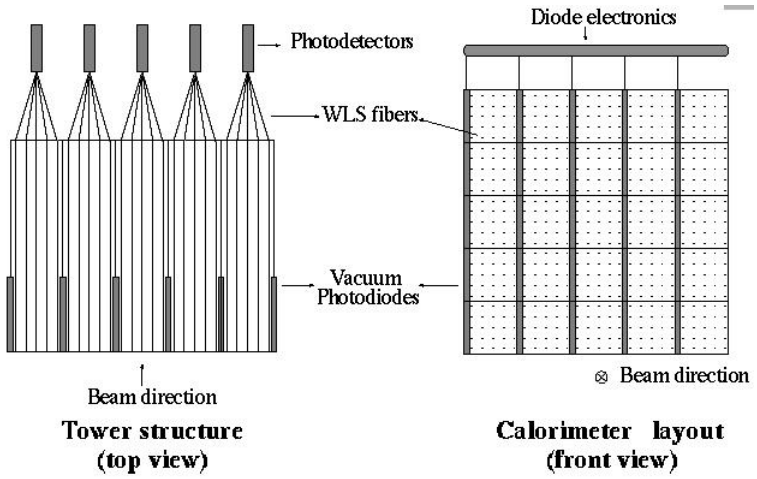

Figure 4.4: Figure of CALIEDOs tower structure. The photodiodes in the figure are connected to an earlier study and can be neglected.

Figure 4.5: The test-beam setup at the CALEIDO test run.

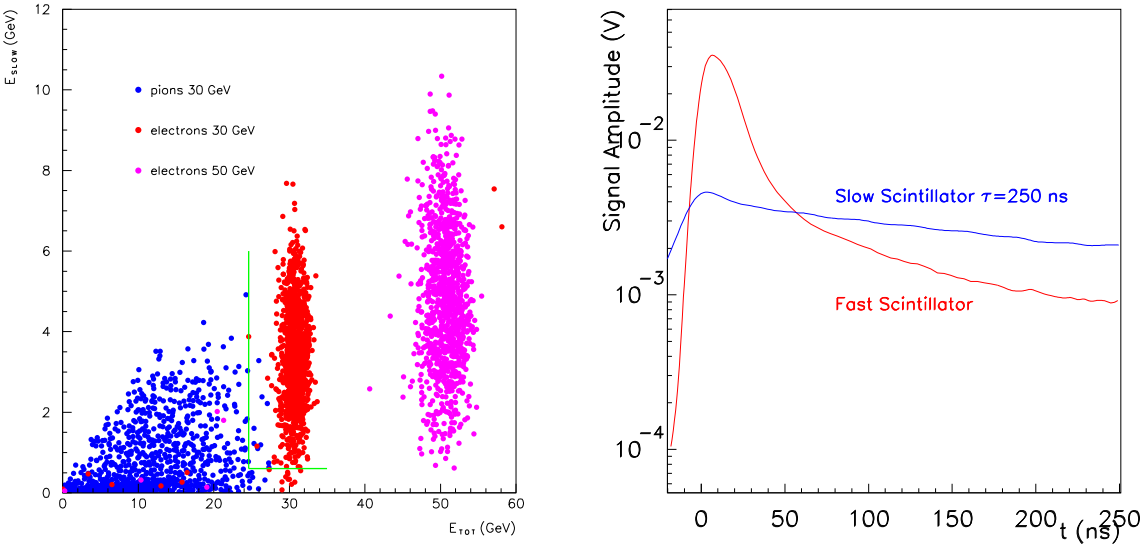

Figure 4.6: Left: Energy in the forward part of CALEIDO versus the total energy for electrons at 30 and 50 GeV and pions at 30 GeV. Right: Time distribution of the signal from the fast and the slow part of the calorimeter.

Any electromagnetic calorimeter can separate pions from electrons by a cut in the measured energy (this is indicated by the vertical line in figure 4.6), since pions only deposit a small part of their energy in an electromagnetic calorimeter. In CALEIDO an additional separation can be obtained by a cut in the energy measured in the slow front part of the detector (the horizontal line in figure 4.6), since pions deposit more of their energy at the back. By using the slow signal the separation capability could be increased by a factor of two.

Chapter 5

Important processes

In this chapter some of the processes used in this study will be discussed.

5.1 Bhabha events

The Bhabha scattering, $e^+e^- \rightarrow e^+e^-$, is used to determine the luminosity at LEP. It is also very useful to study the Bhabha process for other purposes because of its large cross section and the fact that it contains only one detectable electron-positron pair with known energy. The Bhabha process is perfect to study with the STIC calorimeter since

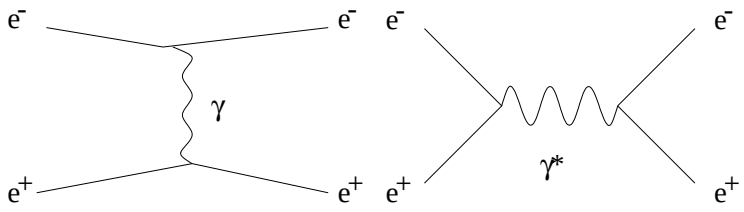

Figure 5.1: t- and s-channel diagrams for Bhabha scattering.

its cross section increases with lower angles.

The differential cross-section can be very well described by second order QED, neglecting the Z^0 corrections:

$$\left(\frac{d\sigma}{d\Omega}\right)_{CoM} = \frac{\alpha^2}{8E^2}\left[\frac{1+cos^4(\frac{\theta}{2})}{sin^4(\frac{\theta}{2})} + \frac{1+cos^2\theta}{2} - \frac{2cos^4(\frac{\theta}{2})}{sin^2(\frac{\theta}{2})}\right]. \tag{5.1}$$

The Bhabha scattering is described, in second order QED, by two different Feynman diagrams. In both of the diagrams the electron and positron are scattered by photons, but the difference is that they are scattered through the so-called t- and s-channel. The t-channel Bhabha event corresponds to the left diagram in figure 5.1, and this photon has a time-like propagation. The scattering through the s-channel then corresponds to the annihilation diagram to the right in figure 5.1, and the photon in this diagram has a space-like propagation.

The three terms in the expression for the differential cross-section comes from the t- and s-channel diagrams. The first term is caused by the t-channel process, and when the angle is small it dominates the Bhabha scattering. The second one comes from the

s-channel process and the third is an interference term between the two diagrams. At small angles one then gets the following differential cross-section:

$$\left(\frac{d\sigma}{d\Omega}\right)_{CoM} \approx \frac{\alpha^2}{8E^2} \cdot \frac{1+cos^4(\frac{\theta}{2})}{sin^4(\frac{\theta}{2})} \approx \frac{4\alpha^2}{E^2} \cdot \frac{1}{\theta^4}. \tag{5.2}$$

Regarding the STIC detector, the total cross-section can then be determined by integrating the differential cross-section over STICs angular region:

$$\sigma_{CoM}^{Tot} = \int_0^1 \int_0^{2\pi} \left(\frac{d\sigma}{d\Omega}\right)_{CoM} d(cos\theta)d\phi = \frac{4\alpha^2}{E^2} \int_{\theta_{min}}^{\theta_{max}} \int_0^{2\pi} \frac{1}{\theta^3} d\theta d\phi = \frac{16\pi\alpha^2}{s} \left[\theta_{min}^{-2} - \theta_{max}^{-2}\right]. \tag{5.3}$$

At $\sqrt{s} = m_Z$ the integrated cross-section for Bhabha scattering in the STIC region is, σ = 61 nb. From these calculations one also gets the differential cross-section

$$\frac{d\sigma}{d\theta} = \frac{32\pi\alpha^2}{s} \cdot \frac{1}{\theta^3}. \tag{5.4}$$

5.2 Radiative events

Radiative processes are very useful for photon studies. A radiative process is when a photon is radiated off the incoming or outgoing particles (figure 5.2).

The most frequent single-photon process predicted by the standard model is a radiative process. It can be seen in figure 5.2 that it contains only one detectable particle, the photon.

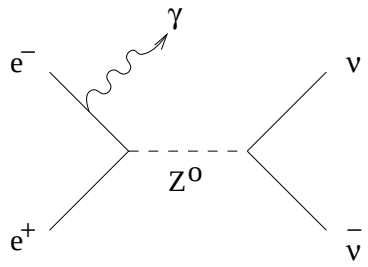

Figure 5.2: Single-photon event.

Another radiative process that was used in this study is the radiative hadronic event shown in figure 5.3. A very useful properity is that the energy of the photon produced in

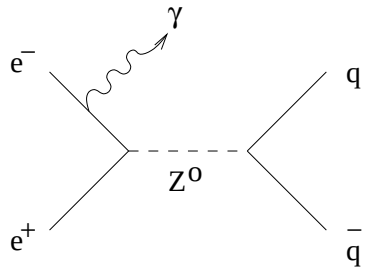

Figure 5.3: Radiative hadronic event.

these events is constant (if the Z^0 is not virtual) and this energy can easily be calculated.

If the rest mass of the electron is negligible compared to the beam energy, and one assumes that the interaction takes place in the same plane, the three particles involved in the early stage of the interaction get the following four-momentum vectors:

$$\overline{P}_{e^-} = \begin{bmatrix} E \\ 0 \\ 0 \\ E \end{bmatrix} \quad \overline{P}_{e^+} = \begin{bmatrix} E \\ 0 \\ 0 \\ -E \end{bmatrix} \quad \overline{P}_{\gamma} = \begin{bmatrix} E_\gamma \\ E_\gamma sin\theta \\ 0 \\ E_\gamma cos\theta \end{bmatrix}. \tag{5.5}$$

One can then calculates the four-momentum of for the Z^0-particle:

$$\overline{P} = \overline{P}_{e^-} - \overline{P}_{\gamma} = \begin{bmatrix} E - E_\gamma \\ -E_\gamma sin\theta \\ 0 \\ E - E_\gamma cos\theta \end{bmatrix} \tag{5.6}$$

$$\overline{P}_Z = \overline{P} + \overline{P}_{e^+} = \begin{bmatrix} 2E - E_\gamma \\ -E_\gamma sin\theta \\ 0 \\ -E_\gamma cos\theta \end{bmatrix}. \tag{5.7}$$

After that one uses the scalar product $\overline{P}_Z \cdot \overline{P}_Z$, which is Lorentz-invariant and equal to the Z-mass squared, to get an expression for the photon energy:

$$M_Z^2 = \overline{P}_Z^2 = (2E - E_\gamma)^2 - |P_Z|^2 = 4E^2 + E_\gamma^2 - 4EE_\gamma - (E_\gamma^2 sin^2\theta + E_\gamma^2 cos^2\theta) \tag{5.8}$$

$$M_Z^2 = 4E^2 - 4EE_\gamma \Rightarrow E_\gamma = \frac{4E^2 - M_Z^2}{4E} \tag{5.9}$$

$$\frac{E_\gamma}{E} = 1 - \left(\frac{M_Z}{2E}\right)^2. \tag{5.10}$$

5.3 Two-photon events

Also two-photon events have been used in this study. The reaction $e^+e^- \rightarrow e^+e^-l^+l^-$, where l stands for lepton, have different contributing processes, such as two interacting virtual photons, bremsstrahlung that produce a lepton pair etc. The first process mentioned, where a photon is radiated off each electron that collides and produces new particles, is the dominating so-called two-photon event. In the events used in this study the collision creates an e^+e^- pair so that there is four electrons/positrons in the final state (figure 5.4).

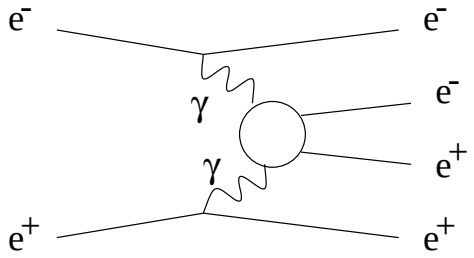

Figure 5.4: Two-photon event.

The two-photon sample that was used in this study consisted of Monte Carlo simulated events, and the sample was made with the BDK generator (Berends, Daverveldt and Kleiss)[11].

Chapter 6

The single-photon analysis

The single-photon analysis is a study where one looks for $e^+e^- \rightarrow \gamma +$ invisible particles. By counting these events one wants to see if there is room for any new physics in the measurements, i.e., if there are more events than predicted by the standard-model, alternatively to set an upper limit on new physics processes at these energies. The standard-model contribution to the single-photon events are radiative events where a Z^0 is produced and decays into a neutrino and an anti-neutrino or were a W-pair is produced and a photon radiated by a beam particle or a W. The single-photon analysis investigates the possibility of additional processes predicted by other models than the standard model. Supersymmetric (SUSY) models predict, for example, final state particles such as neutralinos and gravitinos that are not detected in the DELPHI experiment. Radiative processes with final states containing these particles should contribute to the total number of detected single-photon events. Parameters that have been examined are cross-sections of supersymmetric processes and masses of supersymmetric particles in different SUSY-models.

6.1 Event selection

To select the single-photon events both the tracking detectors and the calorimeters are used. The most important detectors in the selection process are the electromagnetic calorimeters, HPC, FEMC and STIC, which detect the photon. The electromagnetic calorimeters are used together with the tracking detectors in such a way that the tracking detectors confirm that the electromagnetic showers are caused by photons, since no charged tracks are detected. Regarding the STIC detector the veto counters in front of the two STIC modules are used to identify the showers in STIC as electrons or photons. Also HAC is used both to reject cosmic radiation and to separate photons from non-charged hadronic particles. By combining the information from the detectors, the selection of the single-photon events is made basically by requiring one electromagnetic shower in HPC, FEMC or STIC, together with no charged tracks or detected hadrons.

6.2 Background

The largest background to the single-photon analysis is due to the process $e^+e^- \rightarrow e^+e^-\gamma$. This process causes background when the two electrons escape undetected along the beam pipe, or when the electrons are not detected. Since the cross-section of this process

decreases strongly with increasing photon energy, this background can be rejected to a large extent by having an energy cut on the photon shower. Simulations have been made to estimate the remaining background of this process. Another large background in the single-photon analysis is caused by off-energy electrons. The off-energy electrons are, as mentioned before, beam electrons that interact with gas molecules in the beam pipe through the process $e \rightarrow e\gamma$. In this process the photons are always lost in the beam pipe and the electrons are bent by the LEP magnets into the STIC detector, where they appears at low angles. This is the largest background source in the STIC single-photon analysis. Simulations of the off-energy electrons have been made, where it was seen that they were created in certain areas of LEP, and that the magnets in LEP focused them to certain angles. The simulations showed, moreover, that the off-energy electrons appears at the low angles that affect STIC, and that the off-enegy electrons are concentrated in the horizontal plane. The number of off-energy electrons depends on the vacuum pressure in the beam pipe and, since this is not known in detail, the off-energy electron background cannot be estimated by Monte Carlo simulations. Other backgrounds, such as those from two-photon events, have been shown to be negligible.

The problem with the off-energy electron background in the single-photon analysis was the motivation for my study. The first part, the so-called random-trigger analysis, was made to show that a sizable part of background was caused by off-energy electrons, and to determine the amount, but with a trigger that had never been used before. One also wanted to know what the probability was to have an off-energy electron in STIC in any DELPHI physics event.

Since the veto counters in front of the STIC modules are used in the single-photon trigger to select the single-photon events, it is essential to be able to simulate this detector. These simulations have had quite poor accuracy in the past, but are continuously improved. Since the veto counter is used to identify the showers in STIC, as electrons or photons, it is also of great importance regarding the rejection of the off-energy electron background. The second part of my study was to determine the accuracy of the recently improved Monte Carlo simulation of the veto counter.

Chapter 7

The random-trigger analysis

The random trigger is caused by a signal from a scintillator placed close to a radioactive source and this makes a perfect trigger to be used for background and noise measurements.

The advantage of using random triggers compared to triggers from interactions where one has control of the produced particles (back-to-back Bhabha event) is that this makes it possible to study background at lower energies. The disadvantage is a smaller event sample.

There is, however, the possibility that the off-energy electron background is correlated with the interactions and that the random-trigger sample therefore underestimates the off-energy background.

7.1 Analysis tools

The analysis was made using Fortran 77 together with the Skelana package. Skelana is a skeleton analysis programme aimed to be used as a backbone in DELPHI analyses. Skelana fills up standardized common blocks in Fortran 77 with all the data from the different detectors in DELPHI.

To visualize the resulting plots the Physics Analysis Workstation (PAW) package was used. PAW is a programme that provide tools for statistical and mathematical analysis together with different kinds of graphical presentations. It works with objects familiar in physics like histograms, event files, vectors etc and it is also very compatible with the programming language Fortran, which is still the most popular programming language for particle physics analysis. PAW was used to calculate and normalize the different probabilities and error intervals in this study.

7.2 The analysis

The analysis was made in two parts. The first part was a study of what the background in the STIC detector consisted of, and one wanted to confirm that it was caused by off-energy electrons. If so, the next step would be to derive the probability of having an off-energy electron in STIC in an arbitrary event.

The second part was to use the Random Trigger analysis to derive the probability to have a noise/background shower in the other DELPHI calorimeters. In the other calorimeters no further study was made of the cause of the background. The reason for

this was that one expected from simulations of the off-energy electron background that it could not reach the other calorimeters and that the background was caused by either noise or cosmic rays.

7.3 Background in STIC

In principle, the selected STIC showers could be caused by noise and not by off-energy electrons, but this is not the case. Noise in the STIC detector would appear just in one tower, and no showers like this was found with an energy larger than 0.5 GeV (figure 7.1). Another indication that the background is caused by off-energy electrons can be seen in

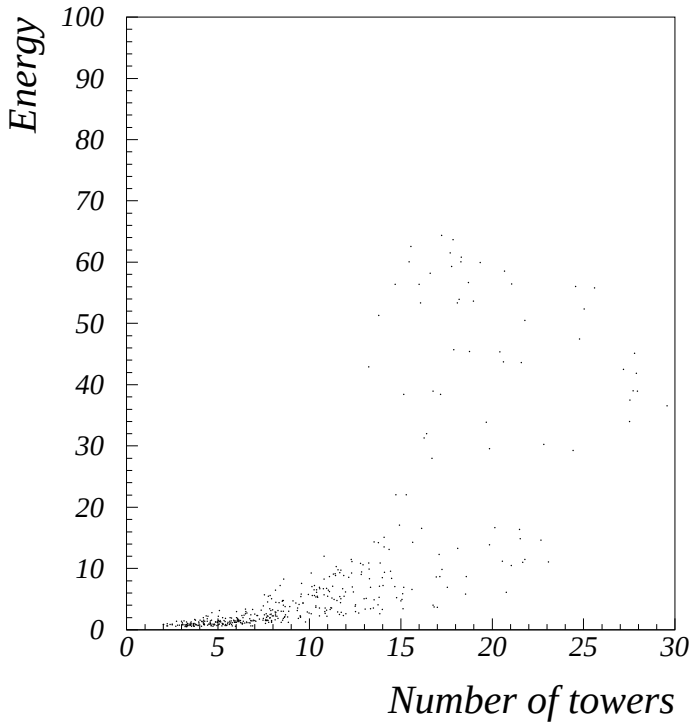

Figure 7.1: The shower energy (GeV) vs. the number of towers that contain the energy.

figure 7.2, which shows a concentration of particles in the horizontal plane. In figure 7.2 one can also see the big difference in the number of particles above and below a polar angle of 3°.

The second goal was to derive the probability of having an off-energy electron in STIC in an arbitrary event. The motivation for this is that the off-energy electrons are such a huge background that they can show up in basically all DELPHI analyses.

When one tries to select single-photon events (figure 5.2), by requiring only one shower in STIC and nothing else, one loses good events because of off-energy electrons giving extra showers. Another problem is when an off-energy electron gives a shower in STIC and is wrongly identified as a photon. This is the largest background in the single-photon analysis. All the particles detected with STIC for this study were required to enter with a polar angle between 2.5° and 8°, because STIC is most accurate in this region.

The probability to have a shower in STIC in a randomly triggered event, as a function of a cut on the STIC energy, is shown in figure 7.3. The figure also shows the probability

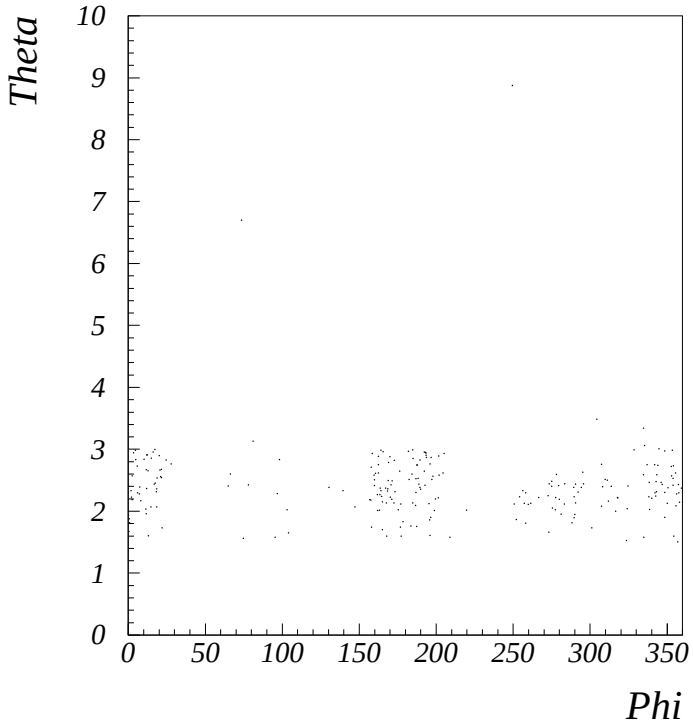

Figure 7.2: The polar angle (θ-Theta) vs. the azimuthal angle (ϕ-Phi) of particles entering STIC.

of having a shower, in a randomly triggered event, that is identified as an electron and for showers with a polar angle larger than 3°. It should be pointed out that one can get off-energy electrons with energies up to 50-60 GeV. Figure 7.3 shows that one can reject a sizable part of the background by requiring that the particle causing the shower should be identified as a electron. The reason for this is that many off-energy electrons enter STIC from the back or from below, and in this case they do not go through the veto counters and they are then identified as photons. Even though this is a good way to reject the off-energy electrons, the best way, as seen in figure 7.3, is to make a polar-angle cut above 3°. Table 7.1 shows a summary of the probabilities of having an off-energy electron in STIC with an energy above E_{min}.

It can be seen in table 7.1 that one out of 100 events in DELPHI has an electron in STIC with an energy larger than 5 GeV. This high rate of electrons can cause problems in many DELPHI analyses. If showers below 3° are discarded this background is reduced by a factor of around 30.

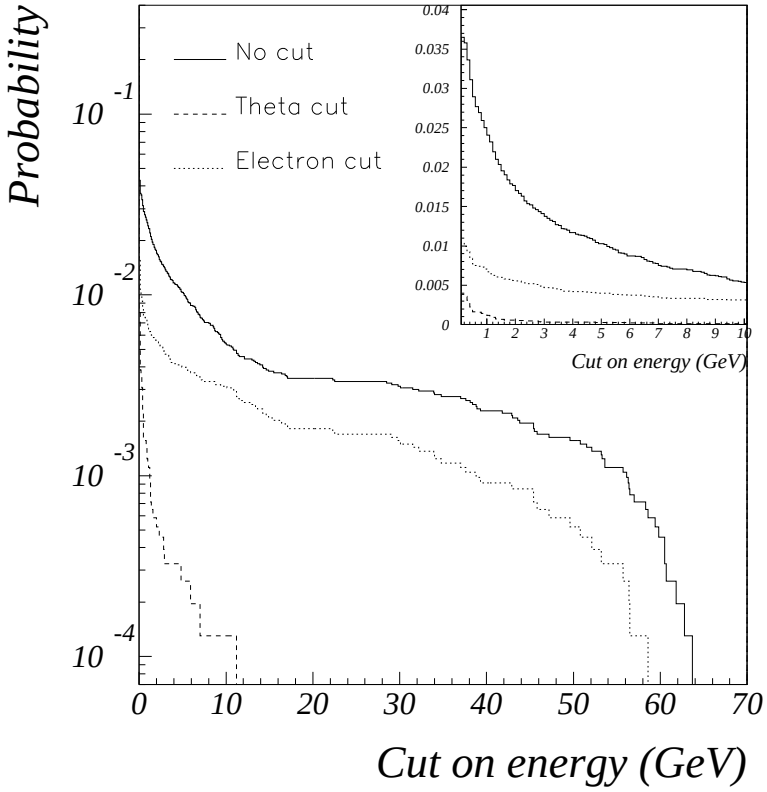

Figure 7.3: Probability to have an off-energy electron in STIC as a function of the energy cut in STIC.

E_{min} (GeV)	P (%)	$P_{\theta>3^\circ}$ (%)
0.1	3.65 ± 0.15	0.39 ± 0.05
0.5	2.89 ± 0.14	0.16 ± 0.03
2.5	1.52 ± 0.10	0.05 ± 0.02
5	1.03 ± 0.08	0.03 ± 0.01
10	0.53 ± 0.05	0.01 ± 0.01
15	0.38 ± 0.05	-
20	0.35 ± 0.05	-
25	0.33 ± 0.05	-
30	0.31 ± 0.05	-
40	0.23 ± 0.04	-
50	0.16 ± 0.03	-
60	0.05 ± 0.02	-

Table 7.1: The probability of an off-energy electron in STIC with an energy larger than E_{min}.

7.4 Noise in HAC, FEMC and HPC

The random trigger was used also to study the other calorimeters in DELPHI. At angles above STIC the calorimeters do not see any off-energy electrons, but they suffer from noise and showers created by cosmic rays. In the 1999 A-processing[1] data noise was

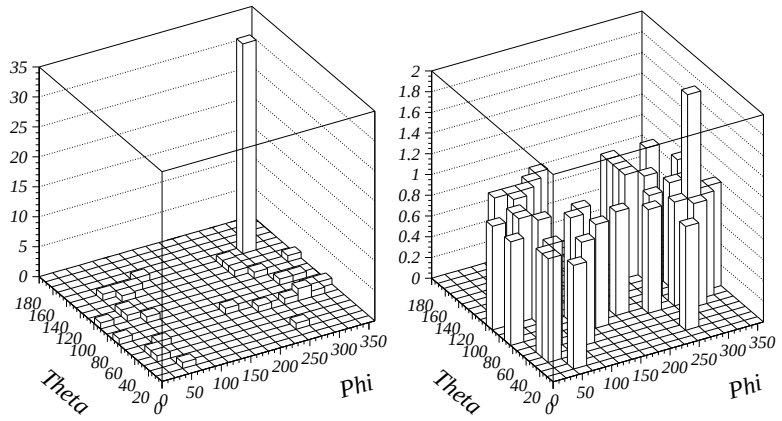

Figure 7.4: The θ (Theta) vs. ϕ (Phi) angle distribution of particles entering HAC. The plot to left the shows the result from the 1999 A-processing data, where noise can be seen. The plot to the right shows the result from the 1999 B-processing data and here it is seen that the noise was removed in the B-processing.

observed in HAC, as the left plot in figure 7.4 indicates. This is shown in figure 7.4 as a large number of showers in a very small area. These noise showers had energies of about 10 GeV (figure 7.5). The results after the B-processing showed that they had been removed (right plot in figure 7.4). Figure 7.6 shows the probability of having a background

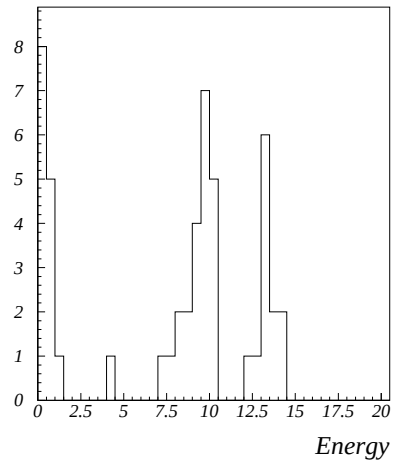

Figure 7.5: The energy distribution of the noise spike in HAC.

shower in the different calorimeters HAC, FEMC and HPC. An important thing to note is that this measurement is useful only for analyses that do not select events based on energy. In FEMC, for example, one sees that the probability to have a background shower with energy larger than 2.5 GeV is extremely small, but if one selects photon events by

[1]See glossary in Appendix A.

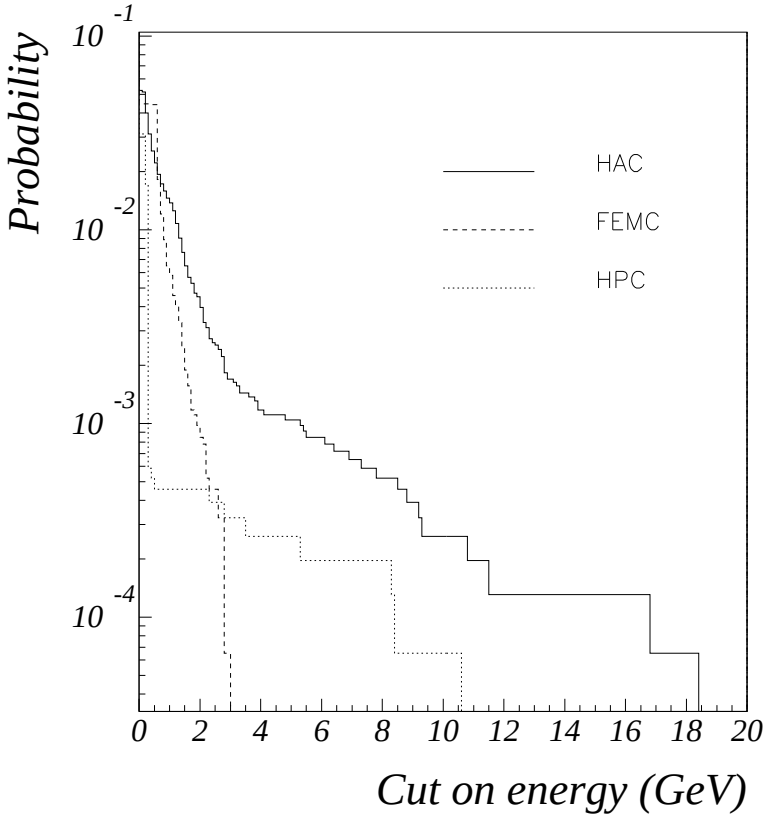

Figure 7.6: The probability to have a noise/background shower in the other calorimeters, HAC, FEMC and HPC, as a function of the energy cut.

triggering on energy in FEMC and requiring that there is no other signals in any other DELPHI detector, the result can be hundreds of single-photon events caused by fake showers. Table 7.2 shows a summary of the different probabilities of having an off-energy electron in HAC, FEMC and HPC with an energy above E_{min}.

E_{min} (GeV)	P_{HAC} (%)	P_{FEMC} (%)	P_{HPC} (%)
0.1	5.15 ± 0.18	4.47 ± 0.17	3.12 ± 0.14
0.5	2.21 ± 0.12	4.42 ± 0.17	0.05 ± 0.02
2.5	0.25 ± 0.04	0.05 ± 0.02	0.04 ± 0.02
5	0.10 ± 0.03	-	0.03 ± 0.01

Table 7.2: The probability of a shower in HAC, FEMC and HPC with an energy larger than E_{min}.

It can be seen that, compared to STIC, the probability is small to have a noise or cosmic shower in HAC, FEMC or the HPC with an energy larger than 5 GeV.

Chapter 8

Monte Carlo simulations of the veto counters

The identification of electrons and photons is of great importance in the study of single photons, and for this reason the STIC detector has been equipped with scintillation counters, called veto counters. As mentioned before, Monte Carlo simulations are important complements to the real data from the different experiments. It is therefore frequently used both to predict physical processes that have not been investigated and to compare with data from the experiments to see how to best select the signal and reject the background.

The Monte Carlo simulation of DELPHI consists of two parts. One part simulates the actual experiment with all the detectors, materials etc and this part is called Delsim. The other part is simulating the colliding particles and what is produced in the collisions. There are many different programmes used for this purpose, and the two used in this analysis are called KoralZ and Pythia.

Monte Carlo simulations of the veto counters have never been used before since they have had quite poor accuracy. Instead efficiency corrections have been made from real measurements, and that works when single particles hit the veto counter. When many particles are produced, as in hadronic events, it does not work that well. Recently Iouri Gouz, from the DELPHI Protvino group, has improved the Monte Carlo simulation of the veto counter. The main things were:

1. Correct the veto counter geometry;
2. Noise that appears in the detectors, called Pedestals, were added;
3. The photo-electron and single-electron spectras of the photomultipliers were adjusted;
4. Calibration coefficients were tuned.

The aim of this work was to compare the Monte Carlo simulation of the large veto counters with real data after these changes.

8.1 The veto counters

As can be seen in figure 8.1, there are two veto counters in front of each STIC calorimeter. They are called the large and the small veto counters. The large veto counters consist of

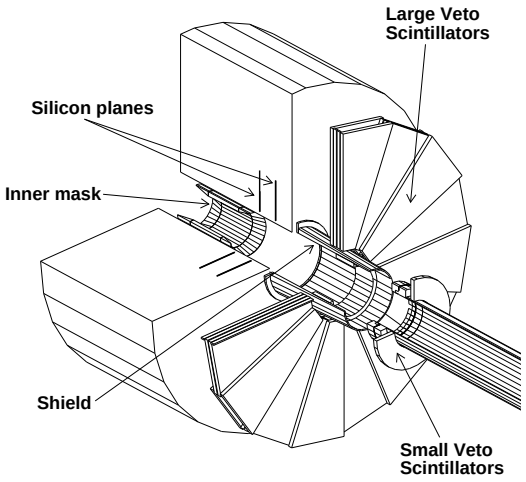

Figure 8.1: Drawing of one of the two STIC calorimeters, together with the large and the small veto counter. The "shield" and "mask" are tungsten rings used to protect the central tracking chambers against low-energy photon background.

two planes of scintillators with each plane divided into 16 segments. The light produced in the scintillators is read out by wavelength shifting fibers connected with optical fibers to photomultipliers. The small veto counters consist of two half-ring shaped scintillators directly mounted on the beam pipe installed during the winter of 1995/1996. The main purpose was to close the gap between the smaller tungsten ring (the "shield" in figure 8.1) used at LEP2 and the lower edge of the large veto counter. It also contributed to a better rejection of off-energy electrons, since they enter at lower angles. The light from the small veto counters are read out in the same way as from the large veto counters, i.e., by wavelength shifting fibers connected to optical cables and then to photomultipliers.

In this study identification of electrons and photons with the large veto counters were made with an identification algorithm that worked as described by figure 8.2. A particle is identified as an electron if both scintillator planes give a signal. Otherwise the particle is identified as a photon. The photon identification is divided into two categories; tight and loose photons. A particle is identified as a tight photon if there is no signal in any of the scintillator planes, and a loose photon if there is a signal in one of the planes.

8.2 The analysis

Two studies of the Monte Carlo simulation of the large veto counter have been made. The first one was to estimate the efficiency of the electron identification, and the second was to estimate the efficiency of identifying photons.

The study was made in Fortran 77 together with the Skelana programme package. In the Skelana programme a common block containing the data produced by the large

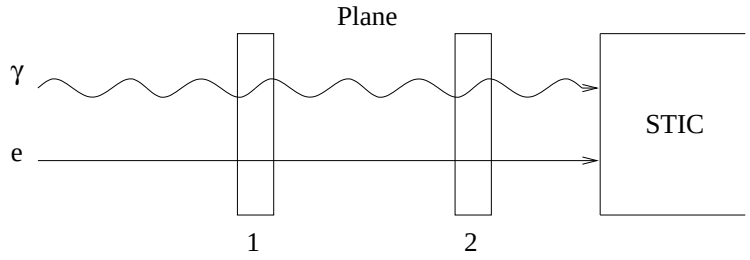

Electron, e	=	Signal	&	Signal
Loose Photon,γ	=	No Signal	&	Signal
Loose Photon,γ	=	Signal	&	No Signal
Tight Photon,γ	=	No Signal	&	No Signal

Figure 8.2: Selection algorithm for the large veto counter.

veto counter had been implemented earlier (figure 8.3). This common block used the selection algorithm, described above, for the large veto counter. As in the Random Trigger

A.3.3 STIC module information

```
+KEEP,PSCSTC.                    STIC module information
*                              ( PA extra-module SSTC (33) )
*
*    NSTIC                 - Number of tracks with STIC shower  - s f
*    LENSTC                - Length of STIC information
*    QSTIC(LENSTC,MTRACK) - Real    array of STIC information
*    KSTIC(LENSTC,MTRACK) - Integer array of STIC information
*
*    QSTIC( 1,I) - Energy of the shower                        - s f
*    QSTIC( 2,I) - Theta  of the shower                        - s f
*    QSTIC( 3,I) - Phi    of the shower                        - s f
*    KSTIC( 4,I) - Number of towers in the shower              - s f
*    KSTIC( 5,I) - Charged tag from the veto    :              - s f
*         (2)      -2 - tight photon
*         (1)      -1 - loose photon
*                   0 - no information available
*         (3)       1 - electron
*    KSTIC( 6,I) - Silicon strip vertex position               - - -
*
```

Figure 8.3: A part of the skelana manual. This part shows the common block containing the data from the large veto counter.

analysis, all the results were visualized using PAW. PAW was also used to normalize the efficiency/rejection data to their respective event sample and to normalize the Monte Carlo simulated energy distributions to the real ones. This normalization had to be made because the simulations did not correspond to the luminosity of the real data.

The first discovery in this study was that the charged tag given in the common block in figure 8.3 did not correspond to the specifications.

8.3 Electron efficiency and electron rejection

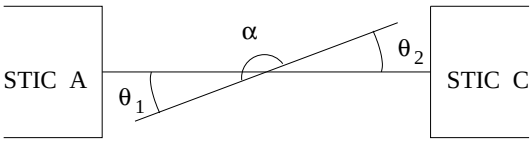

Figure 8.4: The definition of the different angles used in the analysis.

The electron efficiency of the veto counter is given by the fraction of the electrons detected as electrons, and the electron rejection is defined as the fraction of electrons that are wrongly identified as photons. The real data sample that was used in the study of the electron efficiency was back-to-back Bhabha events (figure 5.1). The advantage with these events is first of all that they contain only two electrons. Secondly, they have a very large cross-section, increasing with lower polar angles. The cuts used to select Bhabha events were (the different angles are explained i figure 8.4):

1. Only one particle in STIC on side A and one particle in STIC on side C;
2. $179.85° < \alpha < 180°$;
3. $2.5° < \theta < 8°$;
4. $0.97 < X < 1.05$, where $X = \frac{E}{E_{beam}}$.

The α cut was made after a study of the electron distribution and the peak caused by Bhabha events. It was made to reject the tail caused by radiative Bhabha events. The width of this peak depends only on the calorimeter resolution, and since STIC has a very high resolution this α cut could be made very tight. The θ cuts were made because STIC has its best accuracy between those polar angles. The X cut was chosen after plotting the X-distribution of the events that survived cut 1 to 3.

The Monte Carlo simulated sample was made from a simulation of two-photon events. In the two-photon events studied here an electron-positron pair is produced by the colliding photons, as shown in figure 5.4. The following cuts were made to get a good electron sample:

1. One particle in either STIC on side A or STIC on side C;
2. $2.5° < \theta < 8°$;
3. $0.85 < X < 1.1$, where $X = \frac{E}{E_{beam}}$.

Somewhat looser cuts were made on the X-distribution in the Monte Carlo analysis since it was not necessary to reject radiative events as in the Bhabha selection. The measurement of the electron efficiency is showed in figure 8.5, where the Monte Carlo simulation is compared with the real data. A good agreement is observed and the difference between the data and the Monte Carlo simulation is less than 1%. In this plot the circles represent the Monte Carlo simulation, and the line is the real data. The reason is that the efficiency of the Monte Carlo simulation had much worse statistics than the real data.

The electron rejection measured with the real data was 1.00 ± 0.01 % and with the Monte Carlo data 2.38 ± 0.08 %.

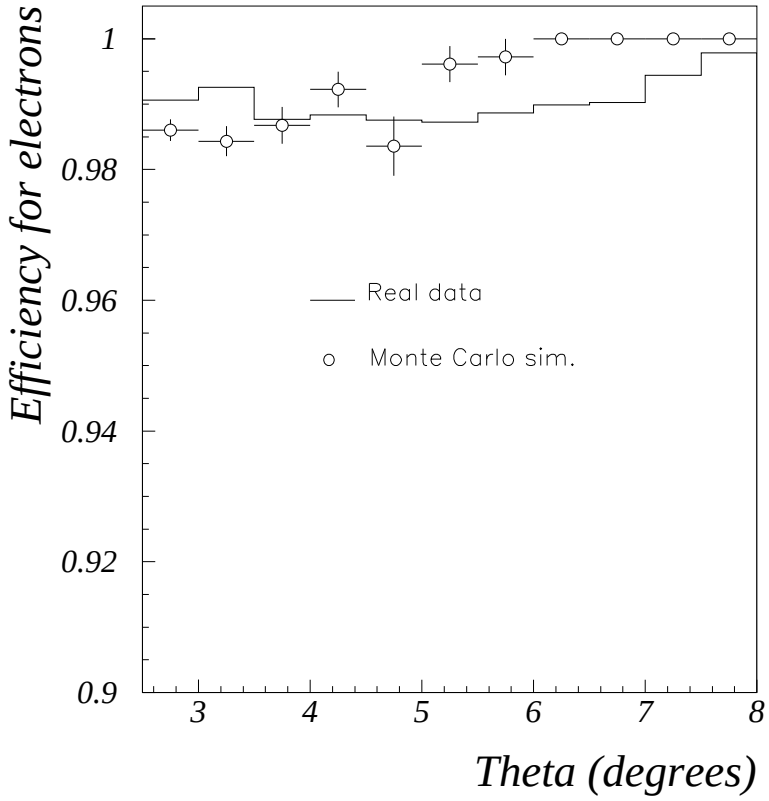

Figure 8.5: A comparision of the efficiency of identifying electrons, with the real large veto counter data and with Monte Carlo data of the large veto counter. The circles are the Monte Carlo simulated data and the line shows the real data.

8.4 Photon efficiency and photon rejection

In the measurement of the photon efficiency both the real sample and the Monte Carlo simulated sample used the photon in hadronic events, such as the one showed in figure 5.3.

The hadronic events were selected with the following cuts:

1. $E_{total} \leq 30\%$ of the centre of mass energy.
   E_{total} is the total energy of the charged particles
   found in the event;
2. More than ten charged tracks per event.

At the average beam energy (96 GeV) of the data one expects a peak at $X \approx 0.77$, according to the calculation in section 5.2. This peak is clearly seen in figure 8.6, showing the energy distribution in STIC.

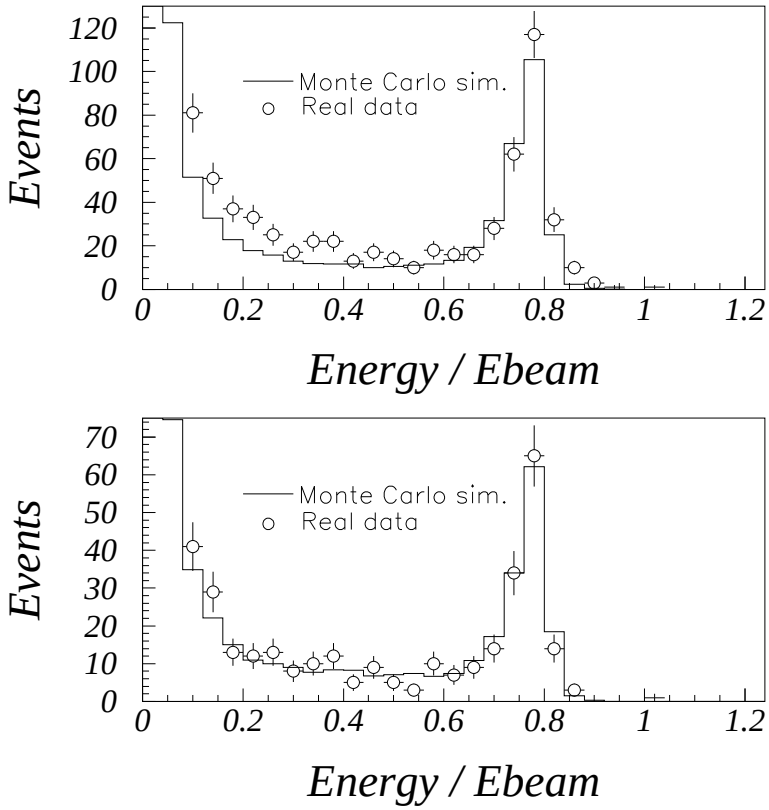

Figure 8.6: Energy distribution of showers in STIC in hadronic events. The upper plot shows the spectra of all showers and the lower plot shows the spectra of showers identified as coming from photons, both as function of the fractional energy $\frac{E}{E_{beam}}$.

It can be seen that at lower energies the curve representing the real data is a bit higher than in the Monte Carlo simulation. This is caused by hadrons, which are not perfectly simulated in STIC by the Delsim programme. Figure 8.6 shows that they are eliminated when the energy distribution of particles identified as photons are plotted. For the study of photon efficiency the photons in this peak were selected with the following cuts:

1. $0.68 < X < 0.84$, where $X = \frac{E}{E_{beam}}$.
2. $2.5° < \theta < 8°$.

Compared to the real data the Monte Carlo simulation from 1998 was in clear disagreement, but the improved simulation from 1999 was not (figure 8.7). The Monte Carlo simulation of 1999 was very good at small angles but somewhat low at larger angles. Even though this affects the peak plotted in figure 8.6 the Monte Carlo simulated peak is similar to the real one because most of the photons are produced at small angles.

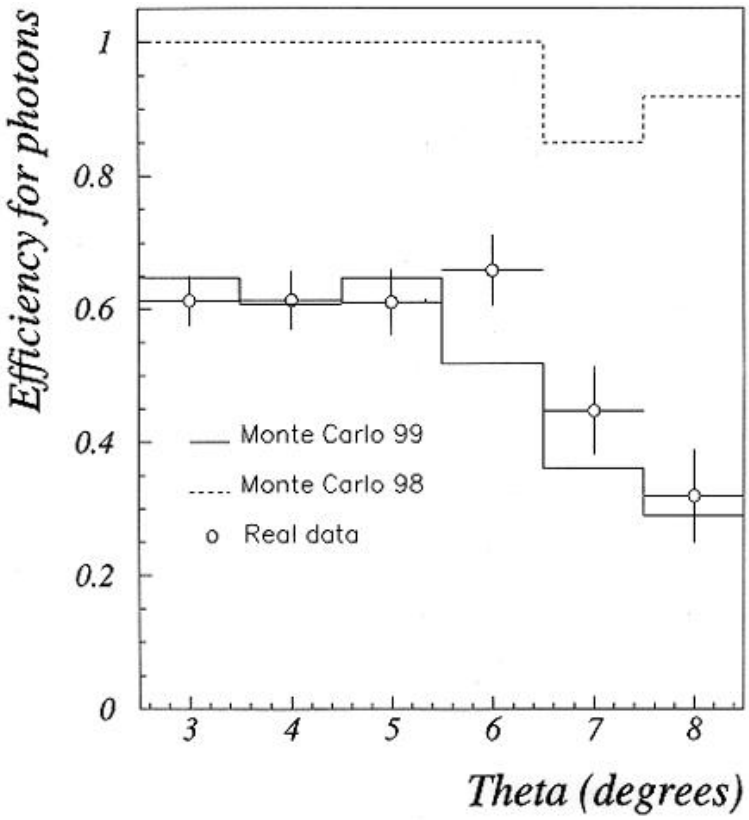

Figure 8.7: The efficiency of identifying photons from the Monte Carlo simulation of the veto counter from 1998, the Monte Carlo simulation of 1999 and from the real veto counter data, as a function of the polar angle θ.

The reason for the difference in efficiency at large angles between the Monte Carlo and the real data was discovered later. The loss of efficiency in the Monte Carlo was due to the material of the laser boxes of the TPC, which was over-dimensioned in the Monte Carlo simulation. The laser boxes of the TPC can be seen in figure 8.8, which shows that they are mounted just in front of the veto counter. Because of the ability of a photon to interact with the material via the photon conversion process, which produces electron-positron pairs, the estimation of the material in the laser boxes is very important for this study. Figure 8.9 shows how the laser boxes are described in the Monte Carlo simulation of the DELPHI experiment (Delsim). Delsim simulates the laser boxes as a solid ring starting at a polar angle of 5.6°. After looking at the drawing of the laser boxes (figure 8.10) it can be seen that this does not describe them in a correct way. The polar angle 5.6° is where the disk, which the laser boxes are attached to, starts. The material that those disks consists of is almost negligible compared to the material of the laser boxes. From the drawing one can see that the actual laser boxes do not start until outside a polar angle of 6.8° and that is quite different from the ring that describes the laser boxes in the Monte Carlo simulation.

This results shows that the improved simulation is almost good enough to be used in a real analysis. The left plot in figure 8.11 compares a Monte Carlo simulation of single-photon events from 1999 with real data, and here the simulation of the veto counter has been used instead of efficiency corrections. As can be seen from figure 8.11 the simulation

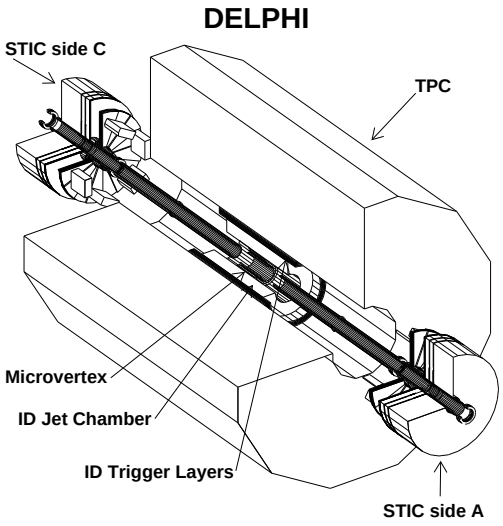

Figure 8.8: Picture of the DELPHI experiment where one can see the TPC laser boxes mounted in front of the veto counter.

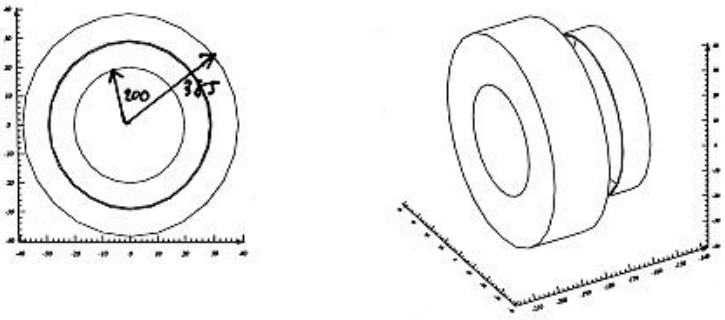

Figure 8.9: The laser boxes as described in the Monte Carlo simulation of the DELPHI experiment.

agrees quite well. The real data consist of 62 events while the simulation (KorlaZ + Delsim) predicts 52.7 events. The problem with the photon efficiency at larger angles could contribute to the lower number of Monte Carlo events. A simulation of single-photon events was made with the simulation of the veto counter plus a correction for the over-estimation of the material in the laser boxes (see right plot in figure 8.11). That simulation predicted 62.8 events, which agrees with the real number (62 events), and this indicates that the wrong estimation of the laser boxes had a 20% effect on the simulation.

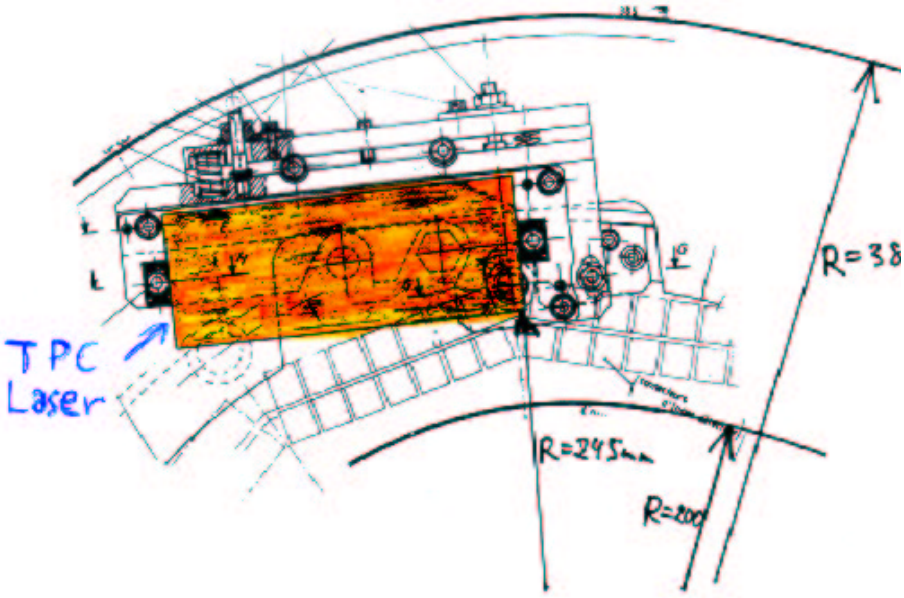

Figure 8.10: Drawing of the laser boxes.

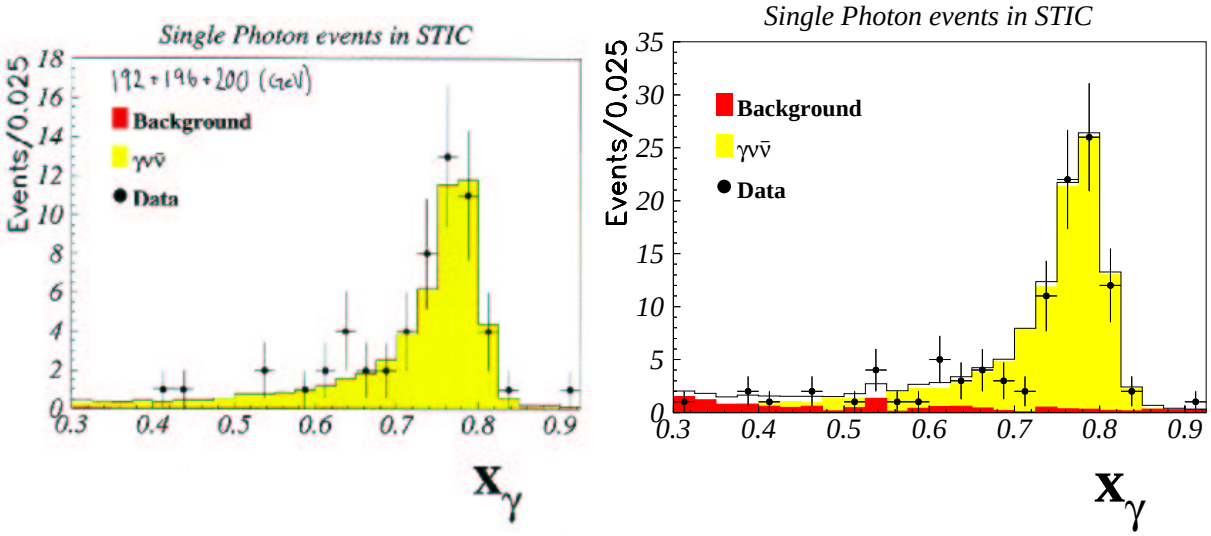

Figure 8.11: Left: Simulation of single-photon events, without corrections for the laser box material, compared with real data. Right: Simulation of single-photon events, with corrections for the laser box material, compared with real data. X_γ is the energy of the photon divided by the beam energy.

Chapter 9

Conclusions

The analysis with the random trigger showed that off-energy electrons were the main source of background in the STIC detector. The probability of having an off-energy electron in STIC with an energy larger than 0.1 GeV is 3.65 $\pm$ 0.15 %. The probability falls with higher energy cuts, but these electrons can cause showers with energies up to 50-60 GeV. The best way of rejecting the off-energy electron background is to make a polar-angle cut at 3°. The results from the random trigger analysis have been compared with earlier studies of the off-energy electrons, and it agrees with the earlier results. As a result of this study most DELPHI analyses are now discarding STIC showers below 3°.

The probability of having noise in the other calorimeters decreased much faster with energy than in STIC. In HPC it was 0.05 $\pm$ 0.02 % already at an energy cut of 0.5 GeV. FEMC had a little bit higher probability of having noise at low energies (4.42 $\pm$ 0.17 % at $E_{min} > 0.5$ GeV), but at an energy cut of 2.5 GeV the probability was 0.05 $\pm$ 0.02 %. The noise in HAC was also sizable at low energies (5.15 $\pm$ 0.18 % at $E_{min} > 0.1$ GeV), but it was lowered to 0.25 $\pm$ 0.04 % at an energy cut of 2.5 GeV. A difference between the noise in HAC, compared to FEMC and HPC, was that it could produce showers with energies of up to 10-15 GeV.

The analysis of the Monte Carlo simulation of the veto counter showed that it has been improved a lot and that it was almost good enough to be used in real physics analyses. The simulation differed from the real veto counter at higher angles, and it was found that the material in the TPC laser boxes, located in this region, was over-dimensioned in the Monte Carlo simulation. When corrections for the over-estimation of the material in the laser boxes were added to the Monte Carlo simulation it showed perfect agreement with the real veto counter data. The Monte Carlo simulation of the veto counter is therefore now used in the real physics analysis after the TPC laser boxes material has been corrected for.

Appendix A

Glossary

The table gives a brief description of some words used in this thesis.

A- & B-Processing	In DELPHI there are programmes, e.g., DELANA and DSTANA, that reconstruct the events from the signals that are read out from the DELPHI detectors. These programmes need calibration data to be able to reconstruct the events with correct energies, positions etc and the calibration files are therefore continuously improved during the year to get more and more precise physics data. The first reconstructed data are called the A-processing data and the data reconstructed later with the improved calibration files are called the B-, C- etc processing data.
Calorimeter	A calorimeter is a particle detector that measures the energy and position of a particle. A calorimeter also destroys the detected particles.
Cherenkov Chamber	A gas chamber where one is able to detect the Cherenkov light emitted by certain particles.
Collimater	Big concrete blocks used to limit the beam size.
Cut	A cut is a limitation of a parameter in an analysis.
Efficiency	Efficiency, in this context, is the number of particles detected compared to the actual number of particles that enter the detector.
EPA	An electron-positron accumulator is a storage device used to collect the particles in order to increase the luminosity.
Luminosity	This is a measure of the collision rate between the particles in the accelerator.
Monte Carlo Simulation	A Monte Carlo simulation is a simulation based on random numbers. The system is described by parameters that weight the random numbers so that the system is simulated with the correct statistical behaviour.
Off-energy electron	An off-energy electron is an electron in LEP that is scattered on a gas molecule in the beam pipe into a detector.
Rejection	Particle rejection is the fraction of particles that escape detection because they are wrongly identified.
Scintillator	A scintillator is a detector consisting of a plastic material that produces light when a charged particle travels through

	it. A scintillator does not destroy the detected particles.
Trigger	A trigger is a device that decides when to make a measurement with a detector. There are both software and hardware triggers, and it is common to combine several triggers to select the desired data.

Bibliography

[1] S. Ask et al., *LEP machine background and noise in the DELPHI calorimeters*, DELPHI 99-157 LEDI 12

[2] E. Falk, V. Hedberg and G. von Holtey, *Simulation of off-energy electron background in DELPHI*, DELPHI 97-12 LEDI 8

[3] P. Ferrari and V. Hedberg, *Photon and electron identification in the very forward region of DELPHI*, DELPHI 98-49 CAL 141

[4] S.J. Alvsvaag et al., *The small angle tile calorimeter in the DELPHI experiment*, CERN-EP/98-132

[5] P. Ferrari et al., *Analysis of the single photon channel at LEP 2*, DELPHI 98-76 CONF 144

[6] *The DELPHI Experiment at LEP*, http://delphi.web.cern.ch/Delphi/index.html

[7] *SL Division*, http://cern.web.cern.ch/CERN/Divisions/SL/welcome.html

[8] B. Povh, K. Rith, C. Scholz, F. Zetsche (1999), *Particles and nuclei, An introduction to the physical concepts*, Springer-Verlag Berlin Heidelberg

[9] F. Mandl and G. Shaw (1996), *Quantum field theory*, John Wiley and Sons Ltd

[10] The L3 collaboration, *Photon structure functions and azimuthal correlations of lepton pairs in tagged $\gamma\gamma$ collisions*, CERN-EP/98-60

[11] The L3 collaboration, *Production of e, μ and τ pairs in untagged two-photon collisions at LEP*, CERN-PPE/97-43

[12] M. Margoni et al., *Shashlik calorimeter prototypes for a linear collider*, submitted to the proceedings of the 1999 IEEE Nuclear Science Symposium, October 26-28, 1999, Seattle, Washington, USA